








A Zone of Preferential Ion Heating Extends Tens of Solar Radii from the Sun

J. C. Kasper^{1,7} , K. G. Klein^{1,8} , T. Weber², M. Maksimovic³, A. Zaslavsky³, S. D. Bale⁴ , B. A. Maruca⁵,
M. L. Stevens⁶ , and A. W. Case⁶ 

¹ Climate and Space Sciences and Engineering, University of Michigan, Ann Arbor, MI 48109, USA; jckasper@umich.edu

² University of Colorado Boulder, Boulder, CO 80309, USA

³ Laboratoire d'études Spatiales et d'Instrumentation en Astrophysique, Observatoire de Paris-CNRS-Université Pierre et Marie Curie-Université Denis Diderot, 92195 Meudon, France

⁴ Space Sciences Laboratory and Physics Department, University of California, Berkeley, CA 94720, USA

⁵ Department of Physics and Astronomy, University of Delaware, Newark, DE 19716, USA

⁶ Harvard-Smithsonian Center for Astrophysics, Cambridge, MA 02138, USA

Received 2017 June 17; revised 2017 July 24; accepted 2017 August 1; published 2017 November 7

Abstract

The extreme temperatures and nonthermal nature of the solar corona and solar wind arise from an unidentified physical mechanism that preferentially heats certain ion species relative to others. Spectroscopic indicators of unequal temperatures commence within a fraction of a solar radius above the surface of the Sun, but the outer reach of this mechanism has yet to be determined. Here we present an empirical procedure for combining interplanetary solar wind measurements and a modeled energy equation including Coulomb relaxation to solve for the typical outer boundary of this zone of preferential heating. Applied to two decades of observations by the *Wind* spacecraft, our results are consistent with preferential heating being active in a zone extending from the transition region in the lower corona to an outer boundary 20–40 solar radii from the Sun, producing a steady-state super-mass-proportional α -to-proton temperature ratio of 5.2–5.3. Preferential ion heating continues far beyond the transition region and is important for the evolution of both the outer corona and the solar wind. The outer boundary of this zone is well below the orbits of spacecraft at 1 au and even closer missions such as *Helios* and *MESSENGER*, meaning it is likely that no existing mission has directly observed intense preferential heating, just residual signatures. We predict that the *Parker Solar Probe* will be the first spacecraft with a perihelion sufficiently close to the Sun to pass through the outer boundary, enter the zone of preferential heating, and directly observe the physical mechanism in action.

Key words: acceleration of particles – magnetic fields – plasmas – solar wind – Sun: corona – turbulence

1. Introduction

Observations of space over the last half century, including spectroscopic diagnostics of UV emission from coronal plasma and direct in situ sampling of solar wind by spacecraft, have shed light on the nonthermal nature of heating in the corona and solar wind. Throughout the heliosphere, plasma is typically found in states other than local thermodynamic equilibrium, with relative drifts and unequal temperatures between species and anisotropic and otherwise non-Maxwellian velocity distribution functions (VDFs) commonly observed. Such nonthermal structure is indicative of mechanisms that selectively couple to particles with particular velocities, charges, or masses and preferentially heat different plasma species. One region in particular where our understanding of these mechanisms is incomplete is the inner heliosphere.

The visible 6000 K photosphere of the Sun is surrounded by a 1–10 MK solar corona that reaches many solar radii (R_s) into space before transitioning into the supersonic and ultimately super-Alfvénic solar wind. The temperature of the solar atmosphere rises to 10^5 K within several hundred km in the

narrow transition region at the base of the corona. At around 0.1 – $0.3R_s$, rising temperatures T and falling densities n are such that the frequency of Coulomb collisions, $\nu_c \propto n/T^{3/2}$, drops to the point that the coronal plasma becomes effectively collisionless, with electrons and individual ion species not persisting in a common local thermodynamic equilibrium. Ions become much hotter than electrons, and heavier ions achieve higher temperatures than the hydrogen that composes the majority of the coronal plasma (Esser et al. 1999; Landi & Cranmer 2009). Emission has been detected from steady nonflare coronal oxygen at $\sim 10^8$ K, 100 times hotter than coronal hydrogen and more than six times hotter than the core of the Sun. Such unequal temperatures serve as a signature of preferential heating of different species in the corona. It is possible that preferential heating is occurring lower in the solar atmosphere, but the higher frequency of Coulomb collisions at lower heights would remove the signature of such heating. The relative temperatures of ion species are highly variable, with a statistical preference for either equal temperatures or equal thermal speeds corresponding to mass-proportional temperatures, but intermediate temperatures and super-mass-proportional temperatures are also observed. For example, a recent study suggested that coronal ions develop an equilibrium temperature $T_i/T_p \approx (4/3)m_i/m_p$ (Tracy et al. 2016). One of the most significant open challenges in solar and space physics is to unambiguously determine the physical processes responsible for this heating.

There are many plausible theories for the physical processes responsible for the extended and preferential heating of different ion species in the corona and solar wind, including

⁷ Smithsonian Astrophysical Observatory, Cambridge, MA 02138, USA.

⁸ Lunar and Planetary Laboratory, University of Arizona, Tucson, AZ 85719, USA.



resonant wave heating (Cranmer 2000; Hollweg & Isenberg 2002), velocity filtration (Scudder 1992), impulsive events including reconnection (Cargill & Klimchuk 2004; Drake et al. 2009), and stochastic heating by low-frequency Alfvénic turbulence (Chandran 2010; Chandran et al. 2010). Unambiguous identification of the dominant process is complicated by uncertainty in the nature of energy readily available for dissipation in the corona. For example, high-frequency waves could escape from the photosphere through the transition region before being damped in the lower corona (Axford & McKenzie 1997). Alternately, MHD turbulence could be generated locally by the interaction between outward and reflected low-frequency waves anywhere below the solar wind Alfvén point (Matthaeus et al. 1999). Recent work (Kasper et al. 2007; Chandran et al. 2013; Kasper et al. 2013) has shown that velocity moments of solar wind H^+ and He^{2+} ions are consistent with both strong heating due to resonant absorption of Alfvén-cyclotron waves or stochastic heating. This heating could persist throughout the heliosphere or occur only in a select region near the Sun, with the resultant nonthermal structure being reduced by infrequent Coulomb collisions as the solar wind expands (Kasper et al. 2008; Tracy et al. 2016). In situ measurements over the last half century, including those from the twin *Helios* spacecraft that approached to within $62R_S$ of the Sun, show that the radial gradients of ion and electron temperatures are much more shallow than would be expected from a cooling solar wind undergoing adiabatic expansion (Hellinger et al. 2013). This evidence for ongoing radial heating in the inner heliosphere is not necessarily evidence for ongoing preferential ion heating of the type observed near the Sun. More detailed tests involving the correlation of particle distribution function structure and electromagnetic fields may be able to identify the energy source and distinguish between the proposed mechanisms (Klein & Howes 2016), but such tests need measurements of the plasma as the heating is occurring. It is therefore important to determine how far away from the Sun the preferential heating mechanism is active, and thus how close to the Sun a spacecraft must approach to directly resolve the process.

In this paper, we address three related questions. Are unequal temperatures in the solar wind maintained by ongoing local preferential heating, or are they a leftover of heating that happened close to the Sun? Is faster solar wind further from local thermodynamic equilibrium than slow wind because only fast wind experiences preferential heating in the corona, resulting in nonthermal structure? How far from the Sun does preferential ion heating continue? The purpose of this paper is to develop a technique for measuring how much time has elapsed since solar wind ions experienced preferential heating that was sufficiently strong to generate super-mass-proportional temperatures. We assume that there is a zone of preferential heating surrounding the Sun, starting at $0.1\text{--}0.3 R_S$, as indicated by spectroscopic observations and ending at an outer boundary R_b . Beyond R_b , any remaining nonpreferential heating is weak and Coulomb collision dominates, leading to an exponential decay of the temperature ratio T_i/T_p toward unity. The observational motivation for this work is presented in Section 2, with a model for the radial evolution of the temperature ratio between H^+ and He^{2+} detailed in Section 3. The technique for measuring the outer boundary of the zone combining the derived model and in situ measurements from the *Wind* spacecraft is presented in Section 4. Values for the outer boundary, discussed in Section 5, are found to be within

the perihelion of the *Parker Solar Probe*, allowing for verification or falsification of our model and, potentially, the first in situ observation of the preferential heating mechanism.

2. Observations of Coulomb Thermalization

The observational basis of this work is an extensive set of measurements of solar wind plasma collected by the Solar Wind Experiment (SWE; Ogilvie et al. 1995) and Magnetic Field Investigation (MFI; Lepping et al. 1995) instruments on the NASA *Wind* spacecraft. *Wind* was launched in late 1994 and has operated continuously in a variety of orbits passing through the solar wind near Earth, resulting in a comprehensive set of observations of solar wind in the ecliptic plane spanning nearly two decades. Solar wind H^+ (protons) and He^{2+} (α -particles) are measured by the SWE Faraday Cup instruments, which record a detailed three-dimensional measurement of the VDF of the two ion species once every 90 s. We use a technique developed to extract anisotropic temperatures and differential flows for each species first described by Kasper et al. (2002). This algorithm makes use of 3 s time-resolution measurements of the vector magnetic field by the MFI flux gate magnetometers in order to determine the temperature of each ion species parallel and perpendicular to the local magnetic field. Approximate uncertainties in the resulting observations were documented in Kasper et al. (2006), which estimated a typical uncertainty in an ion temperature measurement of 8%. We follow the same data selection procedures described in Kasper et al. (2008) but with an additional 8 yr of observations.

Previous work (Feldman et al. 1974; Neugebauer 1976; Livi et al. 1986; Kasper et al. 2008; Tracy et al. 2016) has demonstrated that Coulomb relaxation plays an important role in thermalizing solar wind ions and removing nonthermal structure such as temperature anisotropy and temperature disequilibrium between species. The effect of this thermalization can be quantified by the estimated number of Coulomb thermalization times that have elapsed in the time it takes for the solar wind to expand from the corona to the observing spacecraft, a quantity often referred to as the Coulomb collisional age A_c (Salem et al. 2003; Kasper et al. 2008; Maruca et al. 2013). We will reserve A_c for a more precise calculation presented later in this paper and introduce the Coulomb number $N_C = \nu_{ab}R/U$ to indicate a rough approximation based only on observations at a spacecraft in interplanetary space with no accounting for propagation effects. In this equation, R is the total distance of the spacecraft from the Sun, U is the speed of the solar wind, and ν_{ab} is the characteristic rate for Coulomb interactions between two species a and b ; for N_C , both ν_{ab} and U are assumed to be constant. Throughout this paper, we make use of the calculations of Hernandez et al. (1987) for the Coulomb interaction between two species with Maxwellian distribution functions, different temperatures and densities, and a net differential flow, as discussed in more detail in the following section.

Column-normalized distributions of three markers of non-thermal structure, $T_{\perp p}/T_{\parallel p}$, T_{α}/T_p , and the α -proton drift velocity normalized by the Alfvén speed $\Delta V_{\alpha p}/C_A$, are plotted as a function of solar wind speed U in the left panels of Figure 1. As has been reported many times before, the fast solar wind is more nonthermal than the slow solar wind (cf. Marsch 2012). In the right panels, the same markers are

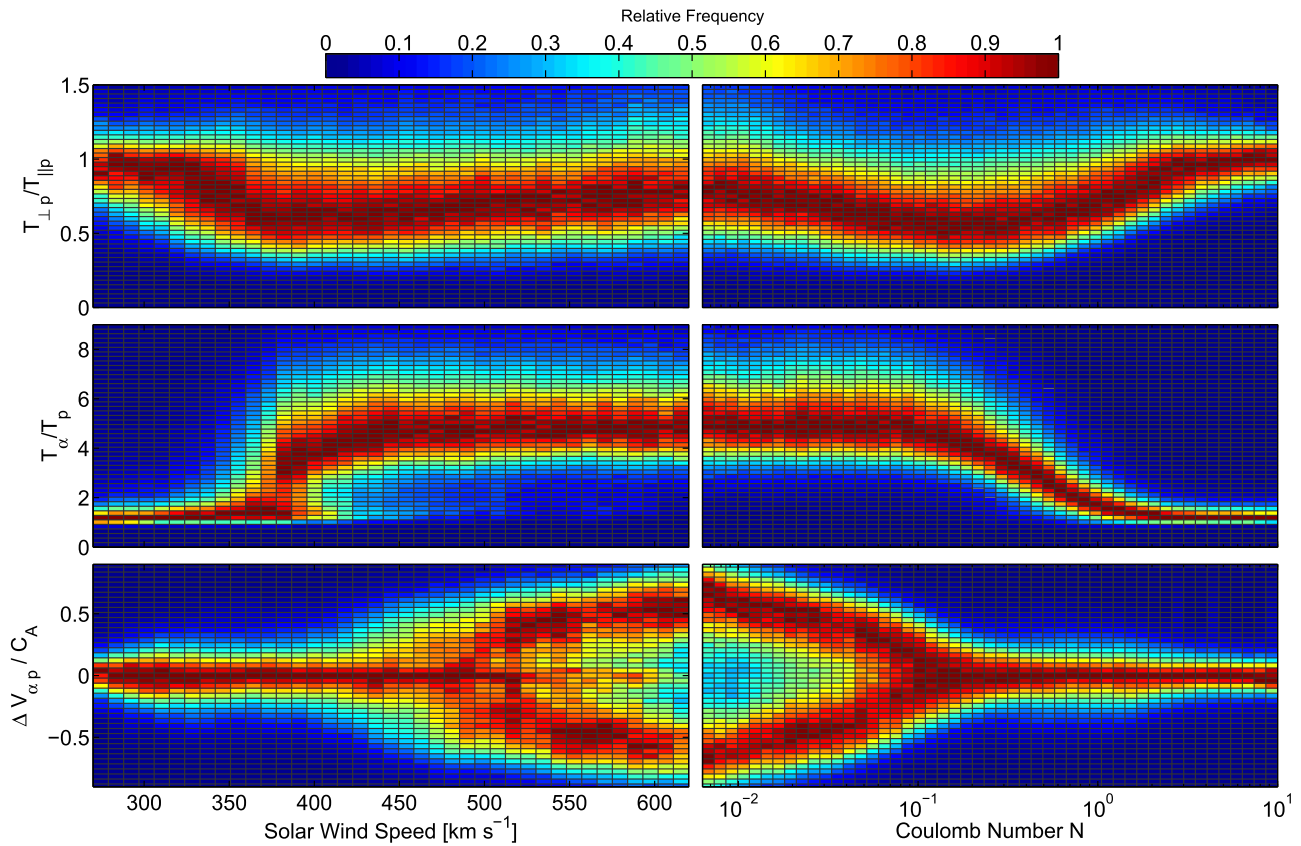


Figure 1. Two-dimensional histograms of the distributions of $T_{\perp p}/T_{\parallel p}$, T_{α}/T_p , and $\Delta V_{\alpha p}/C_A$ as functions of solar wind speed U (left) and Coulomb number N_C (right). While nonthermal solar wind is generally associated with high speeds, these distributions suggest that the occurrence frequency is really determined by the Coulomb number N_C .

plotted as a function of N_C . As previously reported in Kasper et al. (2008), N_C is shown to also order the observations of these three nonthermal measures. The magnitudes of the properties are observed to decrease exponentially with both U and N_C for sufficiently large N_C . For instance, the dependence of T_{α}/T_p on N_C is monotonic, with a single peak value of the temperature ratio for each value of N_C that decreases exponentially with large Coulomb number and a normal distribution of temperature ratios about that peak. The same cannot be said of the dependence of T_{α}/T_p on U ; while it is also strongly correlated, the spread in each T_{α}/T_p is larger and has multiple peaks for a given value of U . In general, the distribution of T_{α}/T_p for a given U is further from a normal distribution than the distribution for a given N_C . The variations of $T_{\perp p}/T_{\parallel p}$ and $\Delta V_{\alpha p}/C_A$ are more complex, possibly because they are more sensitive to kinetic microinstabilities and the effects of expansion, but even so, these nonthermal features are washed away at sufficiently large N_C .

The exponential dependence of T_{α}/T_p on N_C is consistent with a simple model for the radial evolution of the temperature ratio. Considering the thermalization of temperature differences in the absence of any effects other than Coulomb collisions, keeping T_p constant, and following Spitzer (1962), the time evolution of T_{α}/T_p can be written as $d(T_{\alpha}/T_p)/dt = -\nu_{\alpha,p}T_{\alpha}/T_p$, yielding a solution of $T_{\alpha}/T_p \sim \exp[-\int \nu_{\alpha,p} dt]$. Under the oversimplifying but instructive assumption that $\nu_{\alpha,p}$ is constant and the appropriate dynamical time is the transit time from the Sun allows the further simplification $T_{\alpha}/T_p \sim \exp[-N_C]$. This form is in good agreement with the solar wind observations, raising

several interesting possibilities. First, the fact that this single formula fits all of the *Wind* observations across all solar wind speeds suggests that nonunity T_{α}/T_p and preferential ion heating may not be restricted to fast solar wind. Perhaps all solar wind close to the Sun experiences strong preferential ion heating and develops a large T_{α}/T_p , and the apparent association between T_{α}/T_p and U is simply due to the fact that the number of Coulomb collisions a parcel of solar wind experiences varies strongly with U . Slower wind both takes longer to get to the spacecraft and tends to have a significantly higher $\nu_{\alpha,p}$, resulting in a stronger suppression of nonthermal T_{α}/T_p that may be present closer to the Sun. One might counter that T_{α}/T_p and N_C are both strongly correlated with speed or temperature, giving the false impression that N_C regulates T_{α}/T_p . However, Maruca et al. (2013) demonstrated that the temperature ratio has a stronger correlation with the number of Coulomb collisions than other solar wind parameters such as density, speed, and temperature.

To further show that N_C and T_{α}/T_p are not simply dependent on U , we plot in Figure 2 the mean value of the excess temperature ratio $\epsilon \equiv T_{\alpha}/T_p - 1$ as a function of both solar wind speed and N_C . While there is clearly a trend in the typical N_C as a function of speed, the exponential drop in ϵ from high values of ≈ 4 to less than unity happens at all observable speeds at $N_C \sim 0.7$, with a slight dependence on speed. Even the slowest solar wind, with speeds less than 300 km s^{-1} , has high ϵ when N_C is small. As captured in Figures 1 and 2, observations of the solar wind are consistent with a hypothesis that all plasma close to the Sun experiences preferential heating of ions, even plasma that results in slow wind. The association

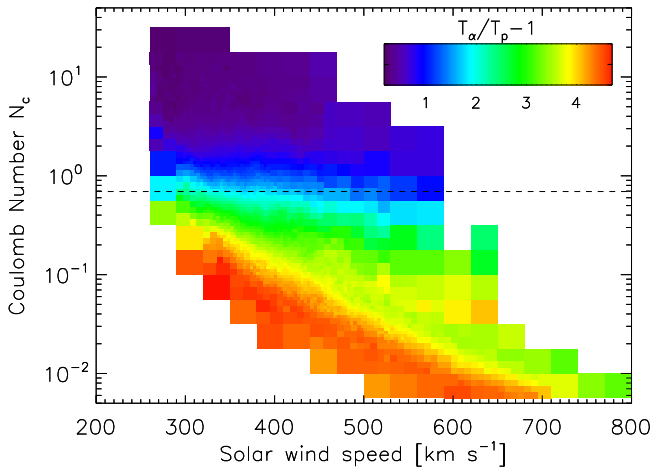


Figure 2. Excess temperature $\epsilon = T_\alpha/T_p - 1$ as a function of the solar wind speed U and Coulomb number N_c . For all solar wind speeds, ϵ decays exponentially with increasing N_c , falling to about half its maximum value near $N_c \sim 0.7$, as one would expect from a simple relaxation process.

of significant ϵ with faster wind speeds is simply due to the fact that slower wind in general has a higher collisional age, leading to a removal of the nonthermal structure by the time the plasma reaches 1 au. This result is significant, because it implies that mechanisms that could produce nonthermal heating may be active in both slow and fast wind. In the following sections, we use this theoretical framework to produce an estimate of how far from the Sun this heating occurred.

3. Modeling the Preferential Heating Zone

The clear exponential dependence of ϵ on N_c in Figures 1 and 2 is suggestive of the gradual thermalization due to Coulomb relaxation on a nonthermal plasma. Spitzer (1962) showed that nonthermal plasma relaxes to thermal equilibrium through a series of small-angle scattering of ions mediated by the Coulomb interaction. In the absence of any other processes, two species with a temperature difference ΔT will come into equilibrium at a rate $d\Delta T/dt = -\nu_c \Delta T$. Ignoring any T dependence in ν_c , we can rearrange this equation as $d\Delta T/\Delta T = -\nu_c dt$ or, integrating both sides and exponentiating,

$$\Delta T = \Delta T_0 e^{-\int \nu_c dt}, \quad (1)$$

where we can define ΔT_0 as the initial temperature difference and the collisional age A_c of the plasma as the integral over time of all Coulomb collisions experienced by the plasma since it began to relax,

$$A_c \equiv \int \nu_c dt \simeq N_c. \quad (2)$$

We now develop a more sophisticated model for the behavior of T_α/T_p , which improves upon the assumption that $\nu_{\alpha p}$ is constant and that the correct dynamical time is the transit time from the center of the Sun to Earth at constant speed, as used for N_c . Such an approach was used in Maruca et al. (2013), which solved the ion temperature differential equations backward in time to investigate the distribution of ϵ near the Sun, finding that for radial distances of 0.1 au, ϵ took on highly nonthermal values for all solar wind speeds. In this paper, we do the opposite: we assume that the plasma is highly nonthermal near the Sun, with a large value of ϵ below some

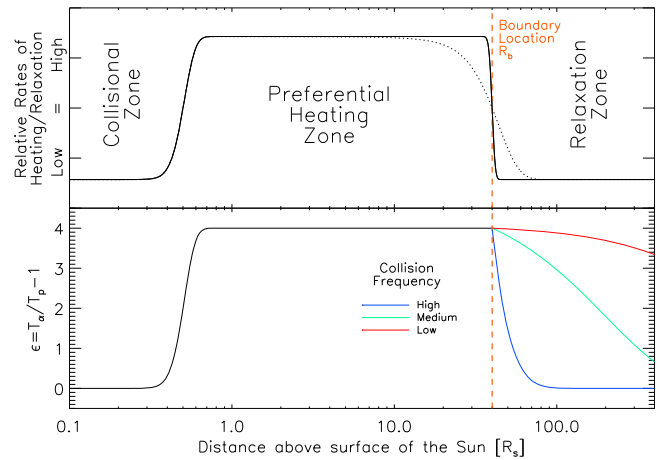


Figure 3. Our simple three-zone model for ion temperature ratios in the inner heliosphere. The upper panel schematically indicates the ratio of the relative rates of preferential ion heating to Coulomb relaxation as a function of distance. The lower panel indicates the resulting excess temperature of He^{2+} relative to H^+ . Close to the surface of the Sun, the plasma is highly collisional and isothermal with $\epsilon = T_\alpha/T_p - 1 = 0$. Above some height, collisions are inefficient, and ϵ rises to an equilibrium value. At the outer boundary R_b , the preferential heating stops, and ϵ decays exponentially with time proportional to the collision frequency. The observed value of ϵ at a spacecraft such as *Wind* is then a function of the equilibrium value in the preferential heating zone and the effects of collisions integrated from R_b to the observer.

radial boundary R_b , and that the observed variation in ϵ at 1 au is subsequently determined solely by Coulomb relaxation. Values for R_b are then obtained from comparing models for radial solar wind behavior with in situ measurements at 1 au.

We make the following key assumptions in the construction of our model, which are illustrated schematically in Figure 3.

1. There is a zone in the inner heliosphere where the Coulomb collision frequency is sufficiently low and the ion heating rate, due to unspecified mechanisms, is sufficiently high to allow for preferential heating of ions. Based on spectroscopic observations of ion temperatures in the corona, this zone begins just 0.2–0.3 R_s above the photosphere, but the outer extent of this zone is unknown.
2. The preferential heating results in different ion temperatures, with ϵ reaching an asymptotic value ϵ_0 within the zone. Here we are motivated by the fact that the observed spread in ϵ is very narrow for small N_c .
3. We assume that at some distance from the Sun, the preferential heating falls off and quickly becomes negligible. We define this outer boundary of the zone as R_b .
4. Above R_b , ϵ decays exponentially as a function of the number of Coulomb collisions.

We acknowledge that this model makes several critical simplifications, each of which merits further investigation. For example, R_b may vary with time, solar wind type, or level of solar activity. The preferential heating, in practice, will not shut off completely at R_b , and it would be worthwhile to investigate the impact of a more gradual evolution. Finally, we know that the steady-state ϵ in solar wind with low A_c is a function of other plasma properties, such as differential flow and plasma β (Kasper et al. 2013), and has a nonnegligible spread for a given set of parameters. Nonetheless, for the purposes of this paper—where we aim to determine if the mean value of the observed temperature excess can be described using a fixed

outer boundary and differentiate between a boundary in the lower corona, interplanetary space, or somewhere in between—this model is sufficient.

To model the excess temperature, we start with an energy equation for T_p and T_α ,

$$\frac{dT_s}{dr} = (\gamma - 1) \left[\frac{T_s}{n_s} \frac{dn_s}{dr} - \frac{Q_s}{n_s k_B U} \right] - \sum_{s'} \frac{\nu_{ss'}}{U} (T_s - T_{s'}), \quad (3)$$

which includes the effects of expansion, input heating, and collisional relaxation. The Coulomb coupling between the ion species is governed by the frequency of energy-changing collisions between the two species $\nu_{ss'}$, and the input heating is parameterized by the heat input rate Q_s in $\text{erg s}^{-1} \text{cm}^{-3}$. This form of the adiabatic energy equation, found, for example, in Cranmer et al. (2009), assumes a steady wind with a radially dependent speed of $U(r)$. Given this form of radial temperature evolution, and assuming the collisional coupling is dominantly between the protons and α -particles, the radial change in ϵ is

$$\begin{aligned} \frac{d\epsilon}{dr} &= \frac{1}{T_p} \frac{dT_\alpha}{dr} - \frac{T_\alpha}{T_p^2} \frac{dT_p}{dr} \\ &= \frac{(\gamma - 1)}{T_p} \left[\frac{T_\alpha}{n_\alpha} \frac{dn_\alpha}{dr} - \frac{T_\alpha}{n_p} \frac{dn_p}{dr} - \frac{Q_\alpha}{n_\alpha k_B U} + \frac{T_\alpha}{T_p} \frac{Q_p}{n_p k_B U} \right] \\ &\quad - \frac{(T_\alpha - T_p)}{T_p} \left[\frac{\nu_{\alpha p}}{U} + \frac{\nu_{p\alpha} T_\alpha}{U T_p} \right]. \end{aligned} \quad (4)$$

To model the excess temperature ratio beyond R_b , we assume that either $Q_s = 0$ for both ion species or any remaining heating affects both species equally. This allows us to relate Q_p and Q_α by

$$Q_\alpha = Q_p \frac{n_\alpha T_\alpha}{n_p T_p}, \quad (5)$$

which, upon insertion into Equation (4), allows us to neglect the input heating terms. We further assume that both ion species follow the same radial density profile,

$$n_s(r) \propto n_{0s} r^{-\xi}, \quad (6)$$

leading to the cancellation of the dn_s/dr terms in Equation (4). With these two assumptions, we have the simplified expression

$$\frac{d\epsilon}{dr} = -\epsilon \left[\frac{\nu_{\alpha p}}{U} + \frac{\nu_{p\alpha}}{U} (\epsilon + 1) \right] = -\frac{\nu_{\alpha p}}{U} [\epsilon(1 + F) + \epsilon^2 F], \quad (7)$$

where we have employed standard expressions for the Coulomb collision frequency between two Maxwellian distributions,

$$\nu_{ss'} = 4\pi q_s^2 q_{s'}^2 \frac{\ln \Lambda n_{s'}}{m_s \mu w_{ss'}^3}, \quad (8)$$

presented in Hernandez et al. (1987) with reduced mass ratio $\mu \equiv m_s m_{s'} / (m_s + m_{s'})$ and the combined thermal speed $w_{ss'}^2 = 2T_s/m_s + 2T_{s'}/m_{s'}$, to write the ratio of collision

frequencies in terms of the mass density ratio

$$\frac{\nu_{p\alpha}}{\nu_{\alpha p}} = \frac{n_\alpha m_\alpha}{n_p m_p} \equiv F. \quad (9)$$

As Tracy et al. (2015) recently demonstrated, for all heavy ions in the solar wind, including He^{2+} , the dominant coupling via Coulomb collisions is with H^+ .

As $\nu_{\alpha p}$ depends on both T_α and T_p , separating ϵ and $\nu_{\alpha p}$ as necessary for a solution to Equation (7) necessitates the construction of a “reduced” collision frequency that only depends on a single temperature,

$$\tilde{\nu}_{ss'} = 8\pi q_s^2 q_{s'}^2 \frac{\ln \Lambda n_{s'}}{m_s^2 w_{s'}^3} = \frac{2\nu_{ss'}}{1 + m_s/m_{s'}} \left(1 + \frac{T_s m_{s'}}{T_{s'} m_s} \right)^{3/2}, \quad (10)$$

where the single-species thermal speed is $w_{s'}^2 = 2T_{s'}/m_{s'}$. Using this reduced collision frequency, we separate Equation (7) into terms that do and do not depend on ϵ , resulting in a differential equation of the form

$$\int_{R_b}^{R_w} \frac{2 \left[1 + \frac{(\epsilon+1)}{4} \right]^{3/2} d\epsilon}{5 \epsilon (1 + F) + \epsilon^2 F} = - \int_{R_b}^{R_w} \frac{\tilde{\nu}_{\alpha p}(r)}{U(r)} dr \equiv -A_c, \quad (11)$$

where our solution depends on integration from the outer boundary of the zone of preferential heating R_b to the radius of the observer R_w .

Expanding the numerator and performing typical u -substitutions, known integral identities, and arithmetic manipulations yields a closed-form expression for the left-hand side of Equation (11),

$$\begin{aligned} \int_{R_b}^{R_w} \frac{2 \left[1 + \frac{(\epsilon+1)}{4} \right]^{3/2} d\epsilon}{5 \epsilon (1 + F) + \epsilon^2 F} &= \frac{1}{10} \frac{\sqrt{5 + \epsilon_w} - \sqrt{5 + \epsilon_0}}{F} \\ &\quad - \frac{\sqrt{5}}{2(1 + F)} \left[\frac{1}{2} \ln \left(\frac{\sqrt{1 + \frac{\epsilon_w}{5}} + 1}{\sqrt{1 + \frac{\epsilon_w}{5}} - 1} \right) - \frac{1}{2} \ln \left(\frac{\sqrt{1 + \frac{\epsilon_0}{5}} + 1}{\sqrt{1 + \frac{\epsilon_0}{5}} - 1} \right) \right] \\ &\quad + \frac{(4F - 1)^{3/2}}{10F^{3/2}(1 + F)} \left[\text{arctanh} \left(\frac{\sqrt{F} \sqrt{5 + \epsilon_w}}{\sqrt{4F - 1}} \right) \right. \\ &\quad \left. - \text{arctanh} \left(\frac{\sqrt{F} \sqrt{5 + \epsilon_0}}{\sqrt{4F - 1}} \right) \right], \end{aligned} \quad (12)$$

where ϵ_0 and ϵ_w are the excess temperature ratio at the outer boundary of the zone of preferential heating and at 1 au, respectively.

A solution for A_c , the right-hand side of Equation (11), requires a description for the radial evolution of the reduced collision frequency $\tilde{\nu}_{\alpha p}$ that depends on the radial structure of n_p , U , and T_p , as well as a value for the boundary R_b . From Equation (10), $\tilde{\nu}_{\alpha p}$ varies as $n_p T_p^{-3/2}$. Both n_p and T_p fall off with distance from the Sun, so it is expected that $\tilde{\nu}_{\alpha p}$ will increase substantially closer to the Sun. Using the radial variations found in *Helios* observations (Hellinger et al. 2013), we take $T_p \propto r^{-\delta}$, $U \propto r^{-\sigma}$, and $n_p \propto r^{-2} U(r)^{-1} = r^{\sigma-2}$. From these scalings, $\tilde{\nu}_{\alpha p}$ as a function of the measured collision

rate at 1 au $\tilde{\nu}_{cp}^w = \tilde{\nu}_{cp}(R_w)$ may be written as

$$\tilde{\nu}_{cp} = \tilde{\nu}_{cp}^w \left(\frac{R_w}{r} \right)^{2-\sigma-1.5\delta}, \quad (13)$$

and thus the collisional age integral is expressed as

$$\begin{aligned} A_c &= \int_{R_b}^{R_w} dr \frac{\tilde{\nu}_{cp}^w}{U_w} \left(\frac{R_w}{r} \right)^{2-2\sigma-1.5\delta} \\ &= \frac{-\tilde{\nu}_{cp}^w}{1-2\sigma-1.5\delta} \frac{R_w}{U_w} \left[1 - \left(\frac{R_b}{R_w} \right)^{-1+2\sigma+1.5\delta} \right]. \end{aligned} \quad (14)$$

Note that care must be taken in evaluating this equation, as a singularity appears for $2\sigma + 1.5\delta = 1$. We note that the assumed scaling relations used for $\tilde{\nu}_{cp}$ may not be accurate, especially close to the Sun, as temperatures in the corona are lower than the extrapolations from the *Helios* trend lines close to the Sun. We will offer a post hoc justification that R_b is sufficiently far from the Sun where these scaling relations serve as accurate descriptions.

Combining Equations (12) and (14) into Equation (11), one can produce a transcendental expression that relates ϵ_w to the measured quantities F , n_p , U , T_p ; fixed parameters δ , σ ; and free parameters R_b , ϵ_0 . Note that rather than determining the parameters that result in ϵ_w approaching zero for high A_c , we allow our solution to relax to a residual ϵ_1 , which is treated as a free parameter in our modeling, to account for the fact that $\epsilon \simeq 0.2$ – 0.3 has been reported even in the case of high A_c both for *Wind*/*SWE* observations of helium and hydrogen temperatures (Kasper et al. 2013; Maruca & Kasper 2013) and for heavier ions (Tracy et al. 2016). It is an open question whether this residual ϵ_1 is indicative of continuing preferential heating acting in interplanetary space at a much reduced weaker level compared to that in the zone of preferential heating or an instrumental measurement error in temperature ratios. The asymptotic value of the temperature excess below R_b in the zone will therefore be $\epsilon_0 + \epsilon_1$. This modeled value ϵ_w will be compared to observed values of ϵ in the fashion described in the following section in an effort to indirectly measure the extent of the zone of preferential heating.

4. Determination of Zonal Boundary Using the *Wind* Data Set

We now describe our procedure for solving for the outer boundary R_b of the zone of preferential heating by comparing our model predictions for the excess temperature ratio with observations of the solar wind by the *Wind* spacecraft. The model is a function of solar wind speed, density, temperature, mass density ratio F , and spacecraft location for each measurement, along with five global free parameters: the boundary height R_b , the steady-state excess temperature ratio within the zone $\epsilon_0 + \epsilon_1$, the residual excess at 1 au ϵ_1 , and the radial exponents of solar wind speed σ and temperature δ . We use observations of the radial dependence of solar wind properties from the *Helios* mission to guide our choice of exponents, since, as we will show, our values for R_b are closer to *Helios* perihelion than to coronal heights where there are spectroscopic measurements. Since there are different reported values for the radial temperature exponent δ in the literature (Marsch et al. 1982; Hellinger et al. 2013), we consider four values of δ , 0.7, 0.8, 0.9, and 1.0, that cover the reported

range. Those same studies have also shown that δ may be a weak function of speed, so the observations were analyzed in separate 25 km s^{-1} intervals in solar wind speed. While Figure 2 clearly shows that the same relaxation of ϵ with increasing Coulomb collisions continues to at least 650 km s^{-1} , we have limited our analysis to the range 300 – 425 km s^{-1} in order to have good observational statistics at high and low A_c with a 25 km s^{-1} interval size. For this work, we keep the solar wind speed exponent fixed at $\sigma = 0$. Observational studies have found negligible dependencies of the solar wind speed on radial distance, with a preference toward a shallow increase in U with r (Hellinger et al. 2011, 2013). As the speed and temperature exponents only appear as a linear combination in the expression for A_c , exploring the dependence of R_b on δ also provides direct insight into the effects of changing σ .

For each range in solar wind speed and assumed value of δ and σ , we now determine the best-fit values of our three free parameters ϵ_0 , ϵ_1 , and R_b by minimizing the χ^2 per degree of freedom difference between the model and the observations, weighted by an error estimate. It might seem that the easiest way to conduct this analysis would be to directly compare the predicted and observed ϵ for every individual observation in a given speed interval. We found that this was unreliable, as Figure 2 shows that there is a very strong preference for a particular collisional age at a given speed. In order to avoid biasing the analysis due to the most common age, we instead histogram our observations into bins in A_c , calculate the mean ϵ in each bin, and compare those means to the model value.

We start with an initial guess for R_b , ϵ_0 , and ϵ_1 . We found that the following analysis is highly insensitive to those initial guesses, but fitting a simple exponential curve to the data provided a good initial guess that speeds up the calculations. For each measurement of ϵ_w , we then calculate an initial collisional age A_c^i using the current values for R_b , ϵ_0 , and ϵ_1 . We also calculate an overall average mass density ratio F using the selected data. The measured ϵ are then binned as a function of the calculated A_c^i , with the range of A_c and the resolution of our bins set up beforehand so that there are always at least 1,000 individual measurements per bin. We use the average over all the selected data. We then calculate a prediction for ϵ_w for each bin using the transcendental expression resulting from Equations (11), (12), and (14). We do not want to use the uncertainty in the mean for each interval in A_c for this analysis, because the high correlation between speed and A_c shown in Figure 2 would strongly bias the best fit to the handful of intervals with the bulk of the observations. Instead, we identified a constant error estimate based on the observed spread of ϵ at very high A_c . We found that at high A_c , the majority of ϵ observations are normally distributed with a width of 7%, and we used this value as the error estimate at all A_c . The nonlinear best fit is thus calculated by variation of R_b , ϵ_0 , and ϵ_1 and iteration of the above binning routine, producing an estimate for the global minimum of χ^2/dof along with the best-fit values and 1σ uncertainties for the three free parameters for each interval of U and value of δ .

Figure 4 illustrates the process and results for three solar wind speed intervals— $U = 300$ – 325 , 350 – 375 , and 400 – 425 km s^{-1} —using $\delta = 0.7$, 0.6 , and 0.8 , respectively. Our simple model of a zone of preferential heating is able to predict the mean excess helium temperature to within 8%–9% with a $\chi^2/\text{dof} = 1.6$ – 1.9 . Typical values for R_b are tens of R_s from the Sun.

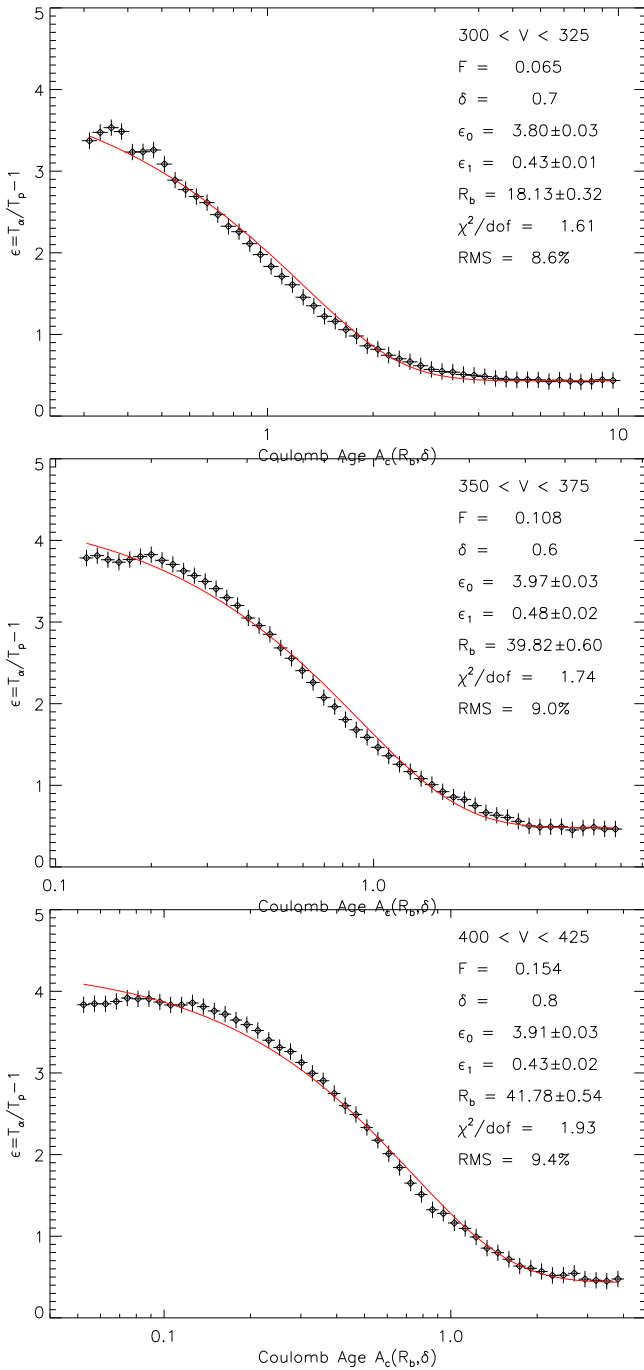


Figure 4. Best-fit match (red lines) of Equation (11) to solar wind observations (diamonds) of helium temperature excess relative to hydrogen for three intervals in solar wind speed. Legends indicate the mean mass density ratio, assumed radial temperature exponent δ , best-fit values for the zone boundary R_b , and excess temperature ratios ϵ_0 and ϵ_1 . Also shown are χ^2/dof and the rms deviation between the model and the observations.

5. Discussion

Following the procedure outlined in the previous section, the best-fit values for R_b as a function of solar wind speed and temperature power-law exponent are calculated and shown in Figure 5. For the value of $\delta = 0.75$, matching the observations of slow wind reported in Hellinger et al. (2013), the outer edge of the boundary ranges from 15 to 40 R_s from the Sun’s surface for varying solar wind speed. The zone boundary is a decreasing function of δ , and, as shown in Figure 6, we see

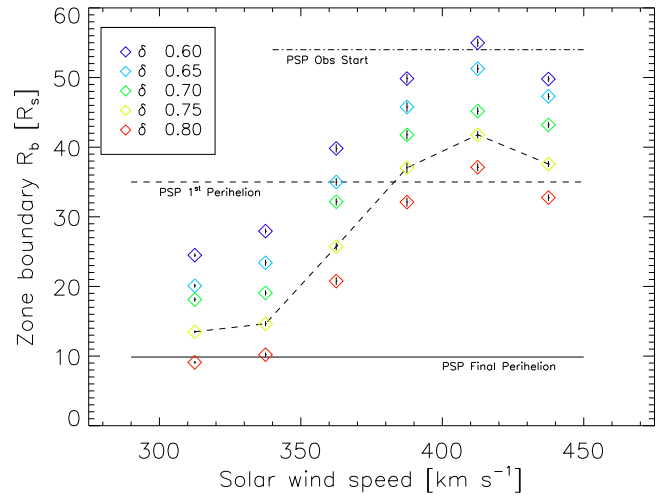


Figure 5. Diamonds with error bars indicate the best-fit values for the outer boundary R_b of the zone of strong preferential heating close to the Sun as a function of solar wind speed and for five different values of the radial temperature power-law exponent δ . Using $\delta = 0.75$ from *Helios* observations in the inner heliosphere, solar winds with speeds from 300 to 425 km s^{-1} experience strong nonthermal heating to an outer boundary 10–35 R_s from the Sun (diagonal dashed line). Horizontal lines indicate the start of science observations (dot-dashed line), the first perihelion distance at the start of the mission (dashed line), and the closest perihelion distance at the end of the mission for the *Parker Solar Probe* (solid line). Based on these results, we predict that the *Parker Solar Probe* will be the first spacecraft to enter and directly observe this zone of preferential nonthermal heating.

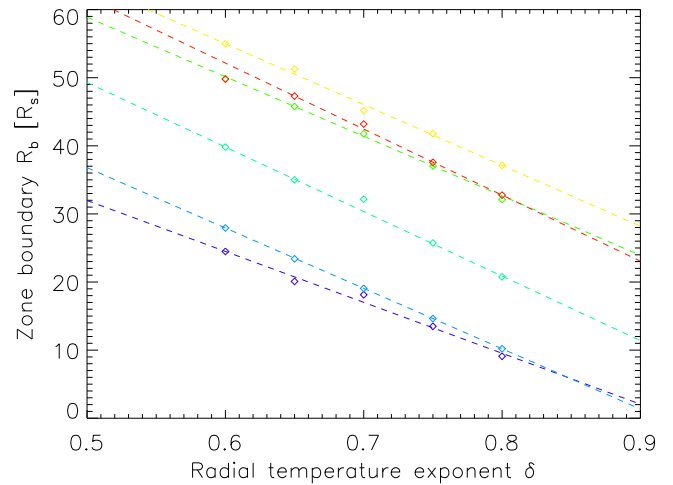


Figure 6. Scaling of best R_b with δ for different solar wind speeds. Colors from purple to red indicate increasing solar wind speed. In general, there is a simple linear dependence between δ and R_b , with the best-fit extent of the zone dropping 8.8 R_s for a 0.1 increase in δ .

that there is a simple linear relationship that allows one to correct R_b for different assumptions of δ , with the dependence of the boundary value on δ fairly independent of speed. Averaging over all the trends shown in Figure 6, R_b drops by 8.8 R_s for every 0.1 increase in δ . Physically, the faster the temperature falls off with distance from the Sun, the smaller the preferential heating zone. Similarly, a linear relation between U and R_b can be found approximately satisfying $R_b \propto 0.1U$ (not shown).

Perhaps the most significant implication of the inferred zone is that the preferential heating does not persist throughout the heliosphere and thus cannot be measured locally by spacecraft at 1 au. Attempts to locally differentiate between proposed

mechanisms for the preferential heating will rely on missions such as the *Parker Solar Probe* (Fox et al. 2015) and *Solar Orbiter* (Müller et al. 2013) that will make measurements of particles and fields in the near-Sun region of the heliosphere (Kasper et al. 2015; Bale et al. 2016). Several key radial distances for the *Parker Solar Probe* mission are shown in Figure 5. All but one of the predicted R_b are below the starting distance for the *Parker Solar Probe* science observations. By the end of the mission, the *Parker Solar Probe* will cross all but one of the predicted values of R_b , allowing direct measurement of the region where the preferential heating is predicted to occur.

We note that our assumption that R_b is sufficiently far away to employ the radial scalings of T_p and U measured by *Helios* has been justified post hoc. Had R_b been on the order of a few R_s , a more sophisticated model for the radial dependence of the collision frequency would have become necessary. Additional modifications to this model, such as the inclusion of the effects of temperature anisotropy or other nonthermal features (Hellinger 2016) on the collision frequency, may have a quantitative effect on the position of R_b , but we expect these effects to be small. Additionally, we will be able to improve our model by using measurements of the radial dependence of n , U , and T by the *Parker Solar Probe* to determine the accuracy of power-law extrapolations from *Helios* observations into the near-Sun environment.

When evaluating this model, one must address the nature of the energy input beyond R_b . While the structure of this model and the best-fit values of R_b indicate that the preferential heating is limited to a region close to the Sun, this does not necessarily imply that no heating persists beyond this region. We know that ion heating on some level extends out to 1 au and beyond (Cranmer et al. 2009), but the rate most likely drops with distance. In the radial model of Chandran et al. (2011), for example, the heating rate is high until about $20 R_s$, and then it falls off as a power law. Our model allows for such heating as long as the heat input per particle for the α -particles satisfies Equation (5). The persistence of a residual, nonzero ϵ even for high- A_c plasma, commented on in Maruca et al. (2013), may be either an indication of a small amount of preferential heating of ions beyond R_b or an instrumental limitation. Characterization of this residual excess temperature ratio will be left to future work.

We think the most plausible interpretation of our results is that R_b is linked to the Alfvén critical point R_A , the radial distance where the solar wind transitions from being sub-Alfvénic to super-Alfvénic, and that the zone of preferential heating is simply the volume of space below the Alfvén point where reflected waves traveling back toward the Sun interact with escaping waves to enhance the turbulent cascade and allow it to transport significant energy in the form of intense and counter-propagating fluctuations down to ion kinetic scales. Typical predicted values for R_A lie between 10 and $30 R_s$ (Verdini et al. 2012; Perez & Chandran 2013), consistent with our findings for R_b . Since all sunward-directed Alfvénic fluctuations generated below R_A are trapped below R_A , it is natural to expect that intense reflection-driven turbulence will be stronger in this region (Verdini & Velli 2007).

As a specific example of a preferential ion heating mechanism that would be active below R_A in the presence of counter-propagating ion kinetic scale fluctuations, consider Kasper et al. (2013), which showed that when A_c is small the

dependence of T_α/T_p on plasma β and normalized differential flow speed $\Delta V_{\alpha p}/C_A$ is consistent with heating by counter-propagating Alfvén ion-cyclotron waves (AIC; kinetic scale Alfvénic fluctuations propagating in opposite directions along the local magnetic field), which are significantly more efficient at heating He^{2+} relative to H^+ and, in fact, all other ions heavier than H^+ . In the presence of a spectrum of AIC waves propagating in a single direction, ions heavier than H^+ are slowly heated as resonant scattering diffuses them in velocity space about the phase speed of the waves. If counter-propagating waves are introduced, He^{2+} and heavier ions can scatter off waves traveling in opposite directions, permitting a more general diffusion in velocity space and a far more rapid and preferential heating. A unified explanation of the observations could be as follows. Everywhere below the Alfvén point, counter-propagating Alfvén waves are present and strongly preferentially heat ions heavier than H^+ . This heating is first apparent $0.1\text{--}0.3 R_s$ above the surface of the Sun when the Coulomb collisions are no longer able to prevent temperature differences from emerging. From that height up to the Alfvén point, all ions are heated by these counter-propagating waves and diffuse in phase space to reach an equilibrium temperature excess. Suddenly, at the Alfvén point, reflected waves are not able to travel back toward the Sun, and the power in counter-propagating waves drops significantly, shutting off the counter-propagating AIC mechanism. The temperature excess developed below the Alfvén point then decays through Coulomb relaxation to the level observed at an interplanetary spacecraft. This sharp drop in heating at R_A is consistent with our assumption that heating stops at R_b and could help explain why our simple model for heating with distance fits the observations so well. In this framework, the reason Kasper et al. (2013) could only see their correlations with AIC predictions in low A_c solar wind is because they were never directly observing the heating in action but instead observed a signature frozen into solar wind ions that crossed R_A , and therefore R_b , days earlier. Finally, the small residual temperature excess seen for ions in high- A_c plasma (Maruca et al. 2012; Kasper et al. 2013; Tracy et al. 2016) could then be due to the weaker heating of ions by AIC fluctuations traveling predominantly in one direction.

Another intriguing possibility is that R_b could correspond to the distance recently identified in DeForest et al. (2016) where a transition from relatively steady and laminar radial flow to sheared and turbulently mixed flow is remotely observed. Using an improved analysis of remote observations from the Heliospheric Imager on *STEREO*, the authors identified a region $\sim 40\text{--}80 R_s$ from the solar surface in which the smooth radial expansion of the slow solar wind appears to fragment and break up. As with the Alfvén critical point, the transition in solar wind flow structure reported by DeForest et al. (2016) could signify another boundary in the solar wind that separates different levels of fluctuations and dominant heating mechanisms. Of course, it is also possible that the breakup in smooth flow seen in the images is simply a manifestation of the Alfvén point itself or another height where the Alfvén mach number crosses some value and the plasma becomes unstable.

Lastly, we can use the values for $\epsilon_0 + \epsilon_1$ to look at the implied excess temperature ratio back in the zone of preferential ion heating for direct comparison with coronal heating theories and other observations. Figure 7 shows the coronal excess temperature of helium relative to hydrogen as a

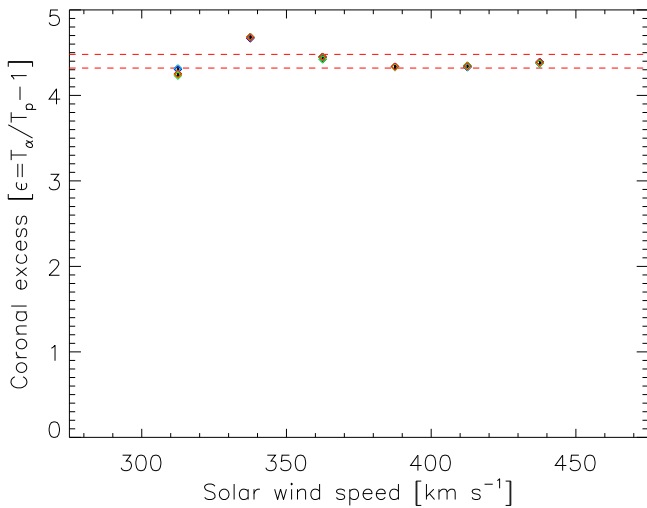


Figure 7. Best-fit values for the excess helium temperature relative to hydrogen $\epsilon_0 + \epsilon_1$ in the zone of preferential heating as a function of solar wind speed. The different colored symbols indicate the assumed value for δ and are indistinguishable, indicating that there is a single steady-state temperature ratio for ions within the preferential heating zone independent of speed. The dashed red horizontal lines indicate the predicted helium excess based on fits to the mass dependence of heavy ions in collisionless solar wind by Tracy et al. (2016), showing that the combined studies are consistent with there being a single super-mass-proportional scaling of $T_i/T_p = (4/3)m_i/m_p$ resulting from preferential heating acting within the zone.

function of solar wind speed and temperature exponent δ , with the symbols for R_b at different δ using the same color scheme as Figure 6. Here we see another significant signature of the physical process responsible for preferential ion heating in the inner heliosphere. Our analysis shows an average temperature excess of about 4.2–4.3, meaning that helium is 5.2–5.3 times hotter than hydrogen, independent of solar wind speed and our assumption for δ . This excess would appear to be a highly significant and model-independent result. Any theory of heating in the corona or extended solar wind should be able to produce this steady-state excess temperature. Finally, we note the dashed red lines in the figure, which were developed by taking the temperature dependency in low A_c or collisionless solar wind reported by Tracy et al. (2016) for heavy ions in the solar wind but evaluated for the mass of helium. We find that within the error reported in that analysis, the implied steady-state helium temperature excess in the corona is consistent with the mass dependence of heavy ions in the solar wind when selecting collisionless wind that presumably indicates the coronal values. We therefore propose that our results, combined with those of Tracy et al. (2016), are consistent with the idea that there is a preferential ion heating mechanism acting in a zone of nonthermal heating that acts on all ions and extends out tens of R_s from the Sun. Within this zone, ion temperatures reach a steady-state ratio of $T_i/T_p = (4/3)m_i/m_p$, independent of solar wind speed.

6. Conclusion

We have examined the temperature ratio of fully ionized He^{2+} and H^+ in the solar wind and its dependence on Coulomb collisional age in order to solve for the location of an outer boundary of an apparent zone of preferential ion heating in the inner heliosphere. Using millions of observations from the *Wind* spacecraft in concert with a physically motivated model for the excess temperature ratio, we are able to construct a best-

fit value for the outer boundary of this region, which falls in the range $\sim 20\text{--}40 R_s$ with some variation with solar wind speed and radial temperature scalings. The restricted radial extent of this region would frustrate attempts to identify preferential heating mechanisms using measurements at 1 au, but future missions, including the *Parker Solar Probe*, will provide measurements both within and outside this region, allowing for the novel measurement of the mechanisms that lead to the nonthermal heating of solar wind minor ions.

We can now answer the three questions proposed in the Introduction. The large unequal ion temperatures seen in situ by spacecraft in the solar wind are not maintained by ongoing local and strong preferential heating. Instead, they are a leftover of heating that happened closer to the Sun. Solar wind at all speeds appears to experience strong preferential heating within our proposed zone, and the only reason fast wind appears more nonthermal than slow wind in interplanetary space is because of the large difference in Coulomb collisions that transpire as the solar wind travels from the outer boundary of the zone to the observing spacecraft. The strong preferential ion heating seen close to the Sun in spectroscopic observations continues $\sim 20\text{--}40 R_s$ from the Sun before dropping off, perhaps due to a lack of counter-propagating Alfvénic fluctuations. It is possible that the residual temperature excess observed in interplanetary space indicates that a weaker form of preferential heating is active outside of the zone, but it is only able to produce temperatures that are different by tens of percent.

The authors acknowledge support from the *Wind* team for the data used for this project. JC Kasper was supported by NASA Grant NNX14AR78G. KG Klein was supported by NASA HSR Grant NNX16AM23G.

ORCID iDs

J. C. Kasper <https://orcid.org/0000-0002-7077-930X>
 K. G. Klein <https://orcid.org/0000-0001-6038-1923>
 S. D. Bale <https://orcid.org/0000-0002-1989-3596>
 M. L. Stevens <https://orcid.org/0000-0002-7728-0085>
 A. W. Case <https://orcid.org/0000-0002-3520-4041>

References

- Axford, W. I., & McKenzie, J. F. 1997, in *Cosmic Winds and the Heliosphere*, ed. J. R. Jokipii, C. P. Sonett, & M. S. Giampapa (Tucson, AZ: Univ. Arizona Press), 31
- Bale, S. D., Goetz, K., Harvey, P. R., et al. 2016, *SSRv*, 204, 49
- Cargill, P. J., & Klimchuk, J. A. 2004, *ApJ*, 605, 911
- Chandran, B. D. G. 2010, *ApJ*, 720, 548
- Chandran, B. D. G., Dennis, T. J., Quataert, E., & Bale, S. D. 2011, *ApJ*, 743, 197
- Chandran, B. D. G., Li, B., Rogers, B. N., Quataert, E., & Germaschewski, K. 2010, *ApJ*, 720, 503
- Chandran, B. D. G., Verscharen, D., Quataert, E., et al. 2013, *ApJ*, 776, 45
- Cranmer, S. R. 2000, *ApJ*, 532, 1197
- Cranmer, S. R., Matthaeus, W. H., Breech, B. A., & Kasper, J. C. 2009, *ApJ*, 702, 1604
- DeForest, C. E., Matthaeus, W. H., Viall, N. M., & Cranmer, S. R. 2016, *ApJ*, 828, 66
- Drake, J. F., Cassak, P. A., Shay, M. A., Swisdak, M., & Quataert, E. 2009, *ApJL*, 700, L16
- Esser, R., Fineschi, S., Dobrzycka, D., et al. 1999, *ApJL*, 510, L63
- Feldman, W. C., Asbridge, J. R., & Bame, S. J. 1974, *JGR*, 79, 2319
- Fox, N. J., Velli, M. C., Bale, S. D., et al. 2015, *SSRv*, 204, 7
- Hellinger, P. 2016, *ApJ*, 825, 120
- Hellinger, P., Matteini, L., Štverák, Š., Trávníček, P. M., & Marsch, E. 2011, *JGR*, 116, A09105

- Hellinger, P., Trávníček, P. M., Štverák, Š., Matteini, L., & Velli, M. 2013, *JGR*, **118**, 1351
- Hernandez, R., Livi, S., & Marsch, E. 1987, *JGRA*, **92**, 7723
- Hollweg, J. V., & Isenberg, P. A. 2002, *JGR*, **107**, 1147
- Kasper, J. C., Abiad, R., Austin, G., et al. 2015, *SSRv*, **204**, 131
- Kasper, J. C., Lazarus, A. J., & Gary, S. P. 2002, *GeoRL*, **29**, 20
- Kasper, J. C., Lazarus, A. J., & Gary, S. P. 2008, *PhRvL*, **101**, 261103
- Kasper, J. C., Maruca, B. A., Stevens, M. L., & Zaslavsky, A. 2013, *PhRvL*, **110**, 091102
- Kasper, J. C., Lazarus, A. J., Steinberg, J. T., Ogilvie, K. W., & Szabo, A. 2006, *JGR*, **111**, 3105
- Kasper, J. C., Stevens, M. L., Lazarus, A. J., Steinberg, J. T., & Ogilvie, K. W. 2007, *ApJ*, **660**, 901
- Klein, K. G., & Howes, G. G. 2016, *ApJL*, **826**, L30
- Landi, E., & Cranmer, S. R. 2009, *ApJ*, **691**, 794
- Lepping, R. P., Acuña, M. H., Burlaga, L. F., et al. 1995, *SSRv*, **71**, 207
- Livi, S., Marsch, E., & Rosenbauer, H. 1986, *JGR*, **91**, 8045
- Marsch, E. 2012, *SSRv*, **172**, 23
- Marsch, E., Rosenbauer, H., Schwenn, R., Muehlhaeuser, K. H., & Neubauer, F. M. 1982, *JGR*, **87**, 35
- Maruca, B. A., Bale, S. D., Sorriso-Valvo, L., Kasper, J. C., & Stevens, M. L. 2013, *PhRvL*, **111**, 241101
- Maruca, B. A., & Kasper, J. C. 2013, *AdSpR*, **52**, 723
- Maruca, B. A., Kasper, J. C., & Gary, S. P. 2012, *ApJ*, **748**, 137
- Matthaeus, W. H., Zank, G. P., Oughton, S., Mullan, D. J., & Dmitruk, P. 1999, *ApJL*, **523**, L93
- Müller, D., Marsden, R. G., St., Cyr, O. C., & Gilbert, H. R. 2013, *SoPh*, **285**, 25
- Neugebauer, M. 1976, *JGR*, **81**, 78
- Ogilvie, K. W., Chornay, D. J., Fritzenreiter, R. J., et al. 1995, *SSRv*, **71**, 55
- Perez, J. C., & Chandran, B. D. G. 2013, *ApJ*, **776**, 124
- Salem, C., Hubert, D., Lacombe, C., et al. 2003, *ApJ*, **585**, 1147
- Scudder, J. D. 1992, *ApJ*, **398**, 299
- Spitzer, L. 1962, *Physics of Fully Ionized Gases* (New York: Interscience)
- Tracy, P. J., Kasper, J. C., Raines, J. M., et al. 2016, *PhRvL*, **116**, 255101
- Tracy, P. J., Kasper, J. C., Zurbuchen, T. H., et al. 2015, *ApJ*, **812**, 170
- Verdini, A., Grappin, R., Pinto, R., & Velli, M. 2012, *ApJL*, **750**, L33
- Verdini, A., & Velli, M. 2007, *ApJ*, **662**, 669